Numerical Modelling of a Free-Burning Arc in Argon. A Tool for Understanding the Optical Mirage Effect in a TIG Welding Device

Jean-Marc Bauchire[*1], Emilie Langlois-Bertrand[1], and Charles de Izarra[1]
[1]GREMI, UMR 6606 CNRS/Université d'Orléans
*Corresponding author: GREMI, Université d'Orléans, 14 rue d'Issoudun, BP 6744, 45067 Orléans Cedex 2, jean-marc.bauchire@univ-orleans.fr

Abstract: In this paper, we present the numerical modelling of a free-burning arc and its application to the understanding of optical mirage effect which could occur in a TIG (Tungsten Inert Gas) device used in welding applications.

Keywords: Argon plasma, electric arc, plasma refractivity, ray tracing, mirage effect.

1. Introduction

Electric arcs are thermal plasmas commonly used in industrial applications as waste treatment, metallurgy, circuit breakers, spraying and coating, cutting and welding… In the simplest configuration, commonly called free-burning arc configuration, arc consists in an electrical discharge of few hundred amps occurring between a flat electrode and a pointed one. The plasma created is composed of electrons, ions and neutral species, at high temperatures (300 K to 25000 K), and it is characterized by a high radiative emission.
The main experimental approach to study this kind of plasma is based on emission spectroscopy [1]. From the spectral analysis of the light emitted by the plasma, it is possible to deduce the characteristics of the arc such as electronic density and temperature. A typical experimental set-up includes optical devices (lens, prism…). It then could be subjected to physical phenomena like optical aberrations. In our case, we have obtained experimental results that suggest the existence of a mirage effect due to the high temperature gradients in the electric arc.
In order to confirm this assumption, we have performed the numerical simulation of our device and ray-tracing in the plasma. After the description of the experimental set-up and the numerical simulation, we present in this paper results of the ray-tracing and the validation of the mirage effect assumption.

2. Experimental Context

The plasma source (TIG Welding device) presented in figure 1 operates with DC current at atmospheric pressure with pure argon. The anode is a copper water cooled disc (diameter 10 cm). The cathode is a water cooled tungsten cylinder of 3.2 mm diameter. During the experiments, the cathode tip is positioned such as it levels the nozzle exit (pink ceramic on figure 1) so that the cathode tip cannot be observed perpendicularly. To obtain a stable plasma column, the distance between the anode and the cathode tip is fixed at 6 mm for an argon flow of 3 Nl/min and a current intensity of 100 A.

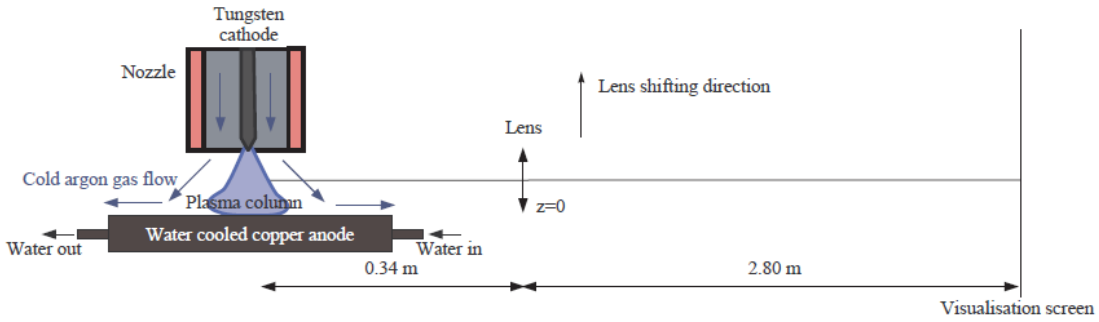

Figure 1. Experimental set-up.

The lens (focal length 30 cm, diameter 42 mm) is moved along the vertical axis. At each lens moving, the cathode length is measured on the visualisation screen. At the beginning of the experiment, the lens optical axe is 3 mm from the anode (z=0 mm). Assuming straight propagation of light, the cathode tip should not be visible when lens position exceed (z = 3 mm) that is to say 6 mm from the anode. However, cathode tip is still visible on the visualization screen for lens shifting of more than 4 cm. This observation suggests that light rays emitted from the cathode tip are bent when passing thought the plasma. The high temperature gradients could imply high refractive index gradient which in turn could deviate light ray. The following arc simulation will allow determining temperature fields in the plasma and then refractive index field. These results will then be used to perform ray-tracing in the plasma to verify the light ray bending.

3. Electric Arc Model

The mathematical modelling of an electric arc needs a multiphysics approach including fluid mechanics, thermal transfer and magnetoelectrodynamics. The corresponding conservation equations are highly coupled, on the one hand implicitly, because all thermodynamic properties and transport coefficients depend strongly on the temperature [2], and on the other hand, explicitly, mainly because the flow depends on electromagnetic forces, temperature depends on Joule effects and electric field is linked to the shape and value of the temperature field.

3.1 General Assumptions

The model is based on the main following assumptions:

- The geometry device is axi-symmetric and then can be described in 2D cylindrical coordinates;
- The flow is laminar and in steady-state;
- The inlet and surrounding gas are argon at atmospheric pressure;
- The plasma is in Local Thermodynamic Equilibrium, i.e. electron and heavy particles have the same temperature;
- Thermodynamic properties and transport coefficients only depend on temperature;
- The net emission coefficient method is used to quantify radiative losses;
- The gravity effect, electrode erosion and electrode sheaths are not taken into account.

3.2 Theoretical model

The positive column of an electric arc is simulated considering flow, energy transfer and electromagnetic phenomena. It is a multiphysics approach with highly coupled equations [2, 3].
Velocity field can be obtained from Navier-Stokes equation, which can be written in our case:

$$\frac{\partial}{\partial z}(\rho vv)+\frac{1}{r}\frac{\partial}{\partial r}(\rho ruv)=-\frac{\partial p}{\partial z}+\ldots$$
$$+\frac{\partial}{\partial z}\left(2\eta\frac{\partial v}{\partial z}\right)+\frac{1}{r}\frac{\partial}{\partial r}\left(r\eta\frac{\partial v}{\partial r}+r\eta\frac{\partial u}{\partial z}\right)+j_r B_\theta$$
$$\frac{\partial}{\partial z}(\rho vu)+\frac{1}{r}\frac{\partial}{\partial r}(\rho ruu)=-\frac{\partial p}{\partial r}+\ldots$$
$$+\frac{\partial}{\partial z}\left(\eta\frac{\partial u}{\partial z}+\eta\frac{\partial v}{\partial r}\right)+\frac{1}{r}\frac{\partial}{\partial r}\left(2r\mu\frac{\partial u}{\partial r}\right)-j_z B_\theta$$

where η is the viscosity, j_z and j_r the current density vector components in axial and radial directions, B_θ the self-induced magnetic field in the azimuthal direction. u and v are the radial and axial velocity components, ρ the mass density and p the pressure.
The temperature field is deduced from the heat equation:

$$\frac{\partial}{\partial z}(\rho C_p vT)+\frac{1}{r}\frac{\partial}{\partial r}(\rho rC_p uT)=\frac{\partial}{\partial z}\left(\kappa\frac{\partial T}{\partial z}\right)+\ldots$$

$$+\frac{1}{r}\frac{\partial}{\partial r}\left(r\kappa\frac{\partial T}{\partial r}\right)+\frac{j_z^2+j_r^2}{\sigma}-4\pi\varepsilon_N$$

where κ is the thermal conductivity, C_p the specific heat at constant pressure, σ the electrical conductivity and ε_N the net emission coefficient. The two last terms of the equation correspond to the Joule heating term and the radiative losses one.

In this case, current density and electric field are deduced from the electric current conservation equation:

$$\frac{\partial}{\partial z}\left(\sigma\frac{\partial \phi}{\partial z}\right)+\frac{1}{r}\frac{\partial}{\partial r}\left(\sigma\frac{\partial \phi}{\partial r}\right)=0$$

where ϕ is the electric potential.
The azimuthal component of the self-induced magnetic field B_θ is deduced from the magnetic potential components (with μ_0 the vacuum permeability):

$$B_\theta=\frac{\partial A_r}{\partial z}-\frac{\partial A_z}{\partial r}$$

and

$$\frac{\partial^2 A_z}{\partial z^2}+\frac{1}{r}\frac{\partial}{\partial r}\left(r\frac{\partial A_z}{\partial r}\right)+\mu_0 j_z=0$$

$$\frac{\partial^2 A_r}{\partial z^2}+\frac{1}{r}\frac{\partial}{\partial r}\left(r\frac{\partial A_r}{\partial r}\right)-\frac{A_r}{r^2}+\mu_0 j_r=0.$$

3.3 Computational Domain and Boundary Conditions

The computation domain is sketched in figure 2. Axisymmetric conditions are set on the centerline (AK).

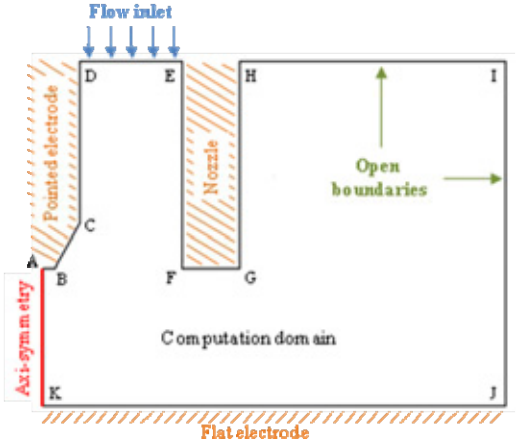

Figure 2. Computation domain.

(ABCD), (EFGH) and (JK) are wall boundaries with no-slip conditions. On the cathode tip, temperature is set to 3000 K - as well as on line (BC). Normal electric current density is imposed on (AB) to fit a current intensity of 100 A. Facing the cathode tip, the line (JK) simulate the anode surface where electric potential is set to 0 (ground condition) and thermal insulation condition is applied for heat transfer. Argon inlet flow, at 300 K, is imposed on line (DE) with a 0.5 $m.s^{-1}$ normal inflow velocity. (HIJ) is an open boundary for which inflow gas temperature equals 300 K. On line (CD), temperature is set to 1000 K, and on the boundary (EFGH), i.e. the ceramic nozzle, a temperature profile is imposed deduced from experimental measurements is imposed. Finally, a condition of magnetic insulation is set on all boundaries for the calculation of the magnetic potential.
The main dimensions are: KJ = 2 cm, IJ = 1.5 cm, AB = 0.5 mm, BK = 6 mm and FG = 2.5 mm.

3.4 Use of COMSOL Multiphysics

The mathematical model presented in section 3.2. is implemented in COMSOL software from the governing equations of the following models:

- Weakly Compressible Navier-Stokes (Heat Transfer Module);
- General Heat Transfer (Heat Transfer Module);
- Meridional Electric and Induction Currents, Potentials (AC/DC Module).

The specific thermodynamic properties (mass density, specific heat), transport coefficients (thermal and electrical conductivity, viscosity), radiative losses and refractive index of argon are all temperature dependent and are previously calculated or taken from the literature [4, 5].
As previously mentioned, these equations are highly coupled and a careful attention is necessary to initiate calculation and to reach convergence.

3.5 Results

Figures 3 to 5 show electric potential, velocity and temperature fields of the plasma. These results are in good agreement with the experimental results of the literature and with those of previous calculations obtained with finite volumes method based software.

The calculated arc voltage concerns only the positive column voltage drop. To compare with arc voltage measurements, it is necessary to add the electrode voltage drops to the value we have obtained. This voltage drop is quite low due to the high temperature and then to the high electric conductivity.

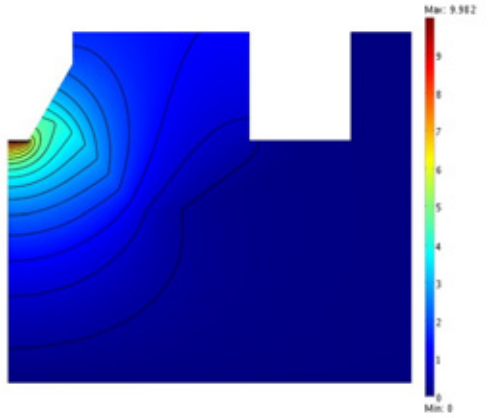

Figure 3. Electric potential field.

The plasma is accelerated on the axis toward the anode and it is also constricted because of the electromagnetic forces. They take part in the stabilization of the plasma column. High temperatures on the axis also contribute the acceleration of the plasma whose maximum velocity is 256 $m.s^{-1}$.

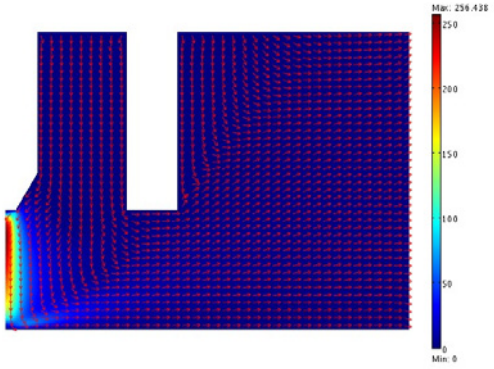

Figure 4. Velocity field and flow direction (arrows).

The plasma temperature reaches 22200 K at the electrode tip because of the high current densities. In this case, electric input power is more than 1 kW. The shape of the isotherms at the anode vicinity depends mainly to the boundary condition. A better simulation of the anode could be obtained considering the entire metallic electrode and performing heat transfer inside.

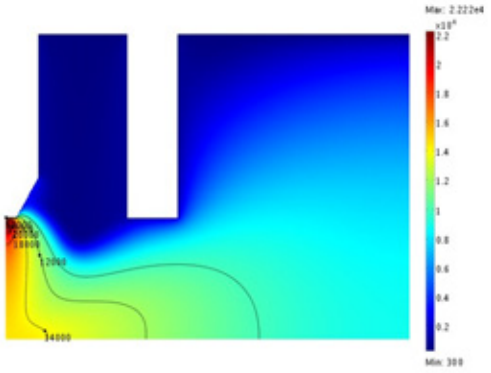

Figure 5. Temperature field.

The refractive index of argon plasma depends in particular on temperature and on the wavelength of interest. Figure 6 show the calculated refractive index versus temperature for a specific wavelength. It can be observed high variations for temperature below 2000 K. It then can be supposed that in this range of temperature notable deviation of light rays could be observed. From the calculated temperature field, and the result of figure 6, we have obtained the refractive index field and the refractive index gradient in the whole domain (figure 7). These results will then be used to calculate the light ray trajectories coming from different parts of the plasma.

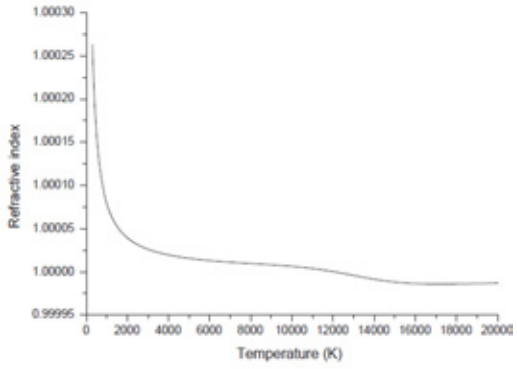

Figure 6. Argon plasma refractive index as function of temperature for λ = 632.8 nm.

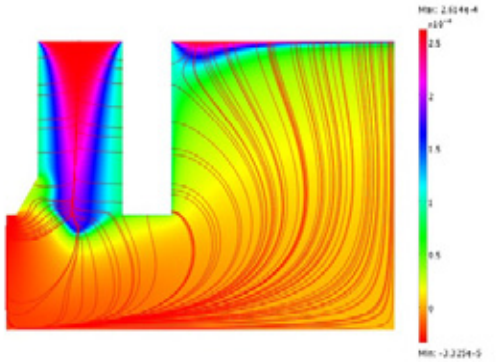

Figure 7. Refractive index field and index gradient (streamlines).

4. Ray-Tracing of the Arc Light

4.1 Ray-Tracing Theory

When rays of light coming from the plasma and the cathode travel through the ionized gas, they cross temperature gradient areas. Therefore, they pass through regions presenting refractive index gradient. Whenever refractive index gradients are large the ray trajectories are significantly deviated.
The ray path in a non homogeneous zone can be calculated with vectorial formulation of Snell-Descartes laws [6]:

$$\frac{d}{ds}\left(n\vec{u}\right) = \vec{\nabla}\left(n\right)$$

where ds is the curvilinear abscissa, $\vec{u}$ the unit vector tangent at any point in the trajectory of the light and n the refractive index. Introducing the terms $dl = \frac{ds}{dn}$, $u_z = \frac{dz}{ds}$ and $u_r = \frac{dr}{ds}$, we have for the arc case:

$$\begin{cases} \frac{d^2 r}{dl^2} = n\frac{\partial n}{\partial r} \\ \frac{d^2 z}{dl^2} = n\frac{\partial n}{\partial z} \end{cases}$$

If the ray of light comes from a point $M_0(r_0,z_0)$ with a θ angle between the cathode axis and the ray propagation direction at M_0 point, we obtained:

$$\begin{cases} \frac{dr_0}{dl} = n_0 \sin\theta \\ \frac{dz_0}{dl} = n_0 \cos\theta \end{cases}$$

This equation system is solved with Euler method.

4.2 Results

Figure 8 and 9 show results of the ray-tracing coming from the arc core and the cathode tip.

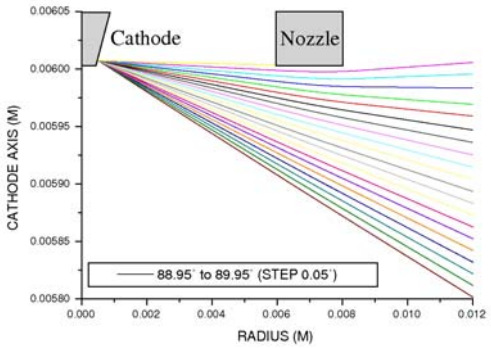

Figure 8. Ray-tracing of light coming from the cathode tip.

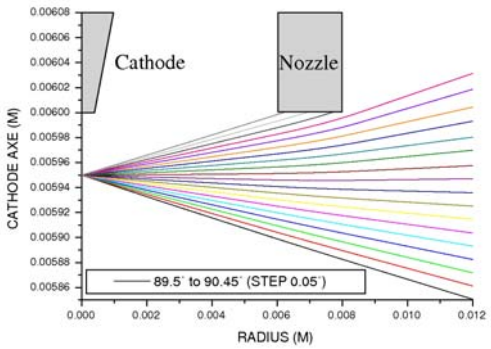

Figure 9. Ray-tracing of light coming from the arc core.

In both cases we can observed that ray trajectories are not deviated when temperature is high. However, at the vicinity of the nozzle, where temperature is between 400 and 3000 K, rays are bent to the top. In this case, cathode can be observed even if observation point is upper

than the nozzle exit. Then these calculations confirm the assumption of optical mirage effect created by warm temperature zone, with special temperature gradient, surely due to the presence of the nozzle.

5. Conclusions

We have used the COMSOL software to simulate the electric arc discharge occurring in a TIG welding device. This numerical simulation has allowed the post-calculation of ray-tracing in the plasma. The results obtained have shown that rays of light coming from the arc core and the cathode tip are deviated, leading to an optical mirage effect that we have observed experimentally.

6. References

1. B Gweon, W Chloe Se Youn Moon and D B Kim, Temperature measurement of an atmospheric pressure arc discharge plasma jet using the diatomic CN molecular spectra, *J. Appl. Phys.*, **105**, 053307 (2009)
2. A B Murphy, M Tanaka, K Yamamoto, S Tashiro, T sato and J J Lowke, Modelling of thermal plasmas for arc welding: the role of the shielding gas properties and of metal vapour, *J. Phys. D: Appl. Phys.*, **42**, 194006 (2009)
3. K C Hsu, K Etemadi, E Pfender, Study of the free-burning high-intensity argon arc, *J. Appl. Phys.*, **54**, 1293 (1983)
4. M I Boulos, P Fauchais and E Pfender, *Thermal Plasmas: Fundamentals and Applications*, Plenum Press, Springer (1994)
5. Y Naghizadeh-Kashani, Y Cressault and A Gleizes, Net emission coefficient of air thermal plasmas, *J. Phys. D: Appl. Phys.*, **35**, 2925 (2002)
6. J P Pérez, *Optique géométrique et ondulatoire*. Ed. Dunod, Paris (1994)